The turbulent near wake of a flat plate at low Reynolds number

Nakayama, A.

Liu, B.

(Citation)
Journal of Fluid Mechanics,217:93-114

(Issue Date)
1990-08

(Resource Type)
journal article

(Version)
Version of Record

(URL)
https://hdl.handle.net/20.500.14094/90001181

J. Fluid Mech. (1990), *vol.* 217, *pp.* 93–114
Printed in Great Britain

The turbulent near wake of a flat plate at low Reynolds number

By A. NAKAYAMA[1] AND B. LIU[2]

[1] Flight Performance, Douglas Aircraft Company, Long Beach, CA 90846, USA

[2] Department of Aerospace Engineering, California State University, Long Beach, CA 90840, USA

(Received 13 July 1988 and in revised form 22 December 1989)

Mean-velocity and turbulence measurements have been made in the turbulent near wake of a flat plate at various Reynolds numbers in order to investigate the low-Reynolds-number effects in this region. The results indicate that the low-Reynolds-number effects are significant enough to partially explain the discrepancies in the existing mean-velocity data. It has been found that, while the Reynolds-number-independent, inner-law similarity of the boundary layers continues to exist, the width of the inner wake that develops within the inner-law region scales with the outer variable. Therefore, the mean velocity near the wake centreline depends on the Reynolds number. It is conjectured that this is due to the influence of the large eddies of the outer layer on the spreading of the inner wake.

Measured turbulence quantities indicate that sudden changes occurring just downstream of the trailing edge are independent of the Reynolds number, but the subsequent development of the turbulent stress profiles depends on the Reynolds number. The Reynolds shear stress and the mean-velocity profiles within the inner wake show approximate similarity.

1. Introduction

Low-Reynolds-number effects on turbulent boundary layers have been experimentally investigated by many researchers, and it is now generally accepted (Coles 1962; Purtell, Klebanoff & Buckley 1981; White 1981; Murlis, Tsai & Bradshaw 1982; Erm, Smits & Joubert 1985) that, as the Reynolds number is reduced, the strength of the wake component decreases as discussed by Coles (1962), but the inner layer is unaffected for values of the Reynolds number based on the momentum thickness R_θ as small as 600. The logarithmic profile exists with a truly constant value of von Kármán's constant κ, but the additive constant C may be slightly Reynolds-number dependent. The direct Navier–Stokes simulation results of Spalart (1988) do not support the experimentally-found behaviour of the wake strength with respect to the Reynolds number, but at least the values of κ deduced from the simulation results are found to be 'essentially unaffected down to $R_\theta \approx 670$'. Numerical computations by Cebeci (1973) using an eddy-viscosity model indicate that good agreement with experimental data can be obtained with Reynolds-number-independent eddy-viscosity parameters in the entire inner layer but with increased values of the eddy-viscosity coefficient in the outer layer.

It is the view of most authors (Bradshaw 1970; Andreopoulos & Bradshaw 1980; Alber 1980; Ramaprian, Patel & Sastry 1982) that, in the near wake of a flat plate, the inner and outer layers of the boundary layers at the trailing edge do not change

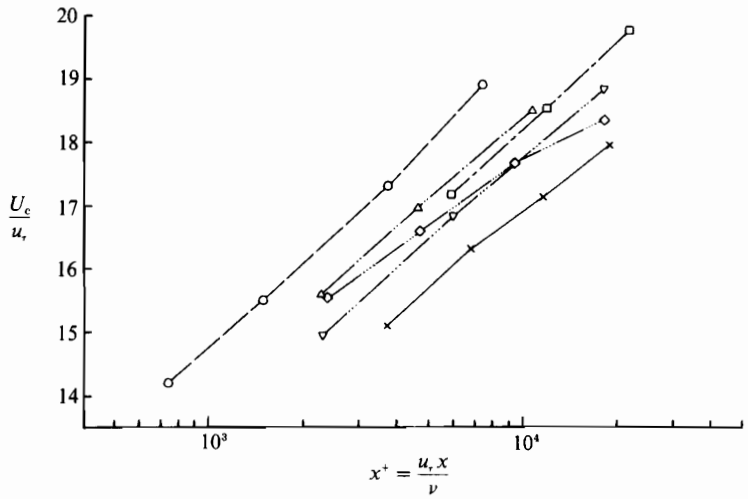

FIGURE 1. Available data of centreline velocity in flat-plate wake. ○, Andreopoulos & Bradshaw 1980, $R_\theta = 13600$; △, Ramaprian *et al.* 1982, $R_\theta = 5220$; □, Pot 1979, $R_\theta = 5880$; ▽, Chevray & Kovasznay 1969, $R_\theta = 1580$; ◇, Akdag 1983, $R_\theta = 1200$; ×, Badri Narayanan *et al.* 1985, $R_\theta = 1200$, slightly asymmetric – the edge-velocity ratio is 0.96.

immediately, but the new thin inner wake evolves from the viscous sublayer as a result of the sudden change in the boundary condition at the trailing edge. Exceptions are the recent analysis of Bogucz & Walker (1987) (also Bogucz 1984) and numerical methods of Chang *et al.* (1986). Bogucz & Walker assume that the entire wall layers of the boundary layers at the trailing edge are replaced by a new inner wake with its own lengthscale that is related to the inner-layer scale of the boundary layer only as an initial condition. Their near-wake model has two layers instead of three, although they do allow an 'initial adjustment region' where the inner wake scale has not grown out of the boundary-layer inner-layer scales. The model of Chang *et al.* (1986) assumes a gradual relaxation to the asymptotic far wake at a constant rate across the entire wake. This is more for computational convenience than physical plausibility. If the view of earlier authors is accepted, the central region of the near wake should be Reynolds-number-independent, just like the inner layers of the upstream boundary layers. In fact, this similarity in terms of the wall variables has been the basis for correlating data (Andreopoulos & Bradshaw 1980; Ramaprian *et al.* 1982) and the assumption in theoretical (Alber 1980) and computational analyses (Cebeci *et al.* 1979; Patel & Chen 1989) of flat-plate wakes. The asymptotic analysis of Bogucz & Walker (1987) for large Reynolds numbers also reduces to the form that is independent of the Reynolds number.

An examination of available data, however, suggests that the near wake data, viewed in terms of the boundary-layer-wall variables, cannot be well correlated. Figure 1 is a plot of the development of the centreline velocity U_c in the symmetric wake of smooth flat plates measured by various researchers (Andreopoulos & Bradshaw 1980; Ramaprian *et al.* 1982; Chevray & Kovasznay 1969; Pot 1979; Badri Narayanan, Raghu & Tulapurkara 1985; Akdag 1983). Both ordinate and the abscissa are scaled by the wall variables of the boundary layer at the trailing edge, such that if a Reynolds-number-independent inner-law scaling applies (as in the inner layer of the boundary layer) the plots must collapse on one curve in the near

wake. Figure 1 shows that this is not the case and that there is a sizeable variation among different sets of data. This variation was pointed out by Ramaprian *et al.* (1982), but no explanation was presented. Figure 1 also shows the general trend of higher U_c/u_τ for higher Reynolds number. Here u_τ is the friction velocity of the boundary layer at the trailing edge. There are, of course, too many uncertainties and non-uniformities among these different sets of data to draw definitive conclusions. For example, effects of the finite trailing-edge thickness and angle may have been significant. In fact, Bogucz (1984) – who based his analysis on some of these data – concluded that there are noticeable effects of the finite trailing-edge thickness in the data of Pot (1979) and Ramaprian *et al.* (1982) and pressure gradient effects in those of Andreopoulos & Bradshaw (1980). The recent data of Haji-Haidari & Smith (1988) fall much higher than any data shown in figure 1. These data seem to be affected too much by the adverse pressure gradient and the thick trailing edge.

The present work was undertaken to examine if the observed trend with respect to Reynolds number is genuine. After confirming that the Reynolds-number effects explain the trend, a more detailed analysis of the data was made. Furthermore, detailed hot-wire measurements were made to document the mean and turbulence data in the near wake of a flat plate at low Reynolds numbers to help clarify underlying physical mechanisms of the low-Reynolds-number effects. The key mechanism is expected to be the way the two boundary layers merge and how the resulting inner wake develops. In the very near wake, the viscous sublayers of the boundary layers start to migrate off the trailing edge subjected to the motions of large eddies. A spectacular visualization of this process has been obtained recently by Haji-Haidari & Smith (1988). Their pictures clearly show 'traces of low-speed fluid' flapping around the wake centreline with streaks of concentrated vorticity. The scales of these structures appear to be related to the outer scales. The conditionally sampled data of Andreopoulos & Bradshaw (1980) further indicate that the intense small-scale mixing continues to exist along the instantaneous interfaces between the two merging boundary layers resulting in the significance of viscosity. Hence the expectation of rather strong Reynolds-number dependence in the near wake is a natural one.

The results show some basic characteristics of the trailing-edge flow at low Reynolds numbers and also have a wide range of applications, including implications for turbulence modelling and interpretations of wind-tunnel-test data taken at low Reynolds numbers. Also, the detailed turbulence data of the low-Reynolds-number turbulent flow in a simple geometry such as the present one should be useful for the development of large-eddy and direct Navier–Stokes simulation methods.

2. Experiments

All experiments were carried out in the low-speed wind tunnel at the Aerodynamics Laboratory of California State University, Long Beach. This tunnel has a test section of 70 cm × 55 cm × 112 cm and a free-stream turbulence level of less than 0.1 % in the range of speed used in the present measurements. Three flat-plate models of aluminium were fabricated with identical leading-edge and trailing-edge geometries, but different overall lengths as shown in figure 2. This figure also shows the definition of coordinates. The total lengths L of these models were 25, 51 and 102 cm. Sandpaper strips of width 12, 25 and 50 mm, respectively, were glued on the model surfaces $\frac{1}{10}$ of the plate length downstream of the leading edge to trip and thicken the boundary layers. The trailing edges were machined into a wedge shape with included

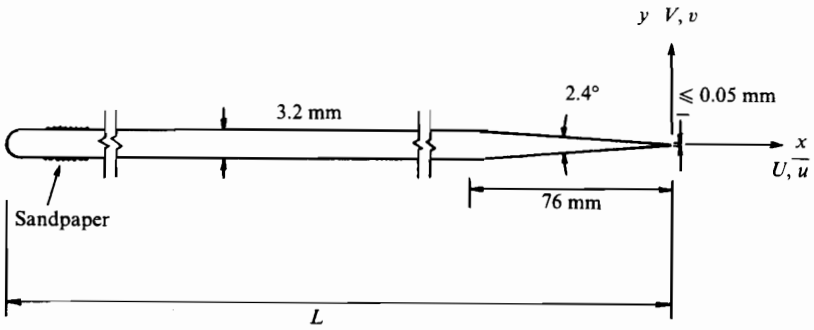

FIGURE 2. Flat-plate models.

Case name	L (mm)	U_e (m/s)	θ (mm) Average in wake	$R_\theta \equiv U_e\theta/\nu$	C_f at $x = 0$	u_τ/U_e at $x = 0$	Symbol in figures 3, 4, 6, 17
L10U40	254	12.2	1.03	812	0.00443	0.0471	◒
L10U80	254	24.4	0.91	1414	0.00375	0.0433	○
L10U160	254	49.0	0.81	2380	0.00343	0.0414	◓
L20U40	508	12.2	1.49	1158	0.00395	0.0444	◨
L20U80	508	24.4	1.37	2112	0.00342	0.0414	□
L20U160	508	49.0	1.22	3619	0.00305	0.0391	◧
L40U40	1016	12.2	2.33	1845	0.00346	0.0416	▲
L40U80	1016	24.4	2.07	3213	0.00303	0.0389	△
L40U160	1016	49.0	1.89	5494	0.00272	0.0369	◭

TABLE 1. Run conditions

angle of 2.4° and hand-finished to a trailing-edge thickness of less than 0.05 mm. Some measurements were also made with a model with slightly thicker trailing edge to examine these effects.

The near-wake characteristics of these flat-plate models were obtained at free-stream velocities of 12, 24, 37 and 49 m/s. The range of the momentum-thickness Reynolds number R_θ obtained was between 800 and nearly 6000. Some combinations of model length and free-stream velocity resulted in nearly the same values of R_θ. These results were useful in assessing the accuracy of the data and the measurement methods which could have been influenced by the velocity and lengthscales of the flow independently. A summary of run conditions is given in table 1.

The problems associated with transition from laminar to turbulent flow and laminar flow instability may be important at very low Reynolds numbers and are not addressed in the present work. The boundary layers at the trailing edge for the lowest-Reynolds-number case presented here are still fully-developed turbulent boundary layers.

The instrumentation used included a small Pitot-tube probe for the measurement of mean velocity and $\times$-wire probes (TSI 1248-T1.0 which were smaller than the regular subminiature probes and had a nominal sensor diameter of 2.5 μm and length of 0.6 mm) for the measurement of turbulence quantities. A small static probe was also used to determine the streamwise variation of the static pressure along the wake

edge. Twin Preston tubes were used to adjust the symmetry and two-dimensionality of the boundary layers at the trailing edge. Pressure measurements were made by Setra Systems 'electronic manometers' together with an Isaac A/D converter operated by a micro computer.

The $\times$-wire probe data were also acquired and analysed by a system based on an Apple computer and an Isaac A/D converter. The method is very similar to that described in Akdag *et al.* (1983). The instantaneous anemometer outputs and the sum and the difference of the two outputs were digitized in real time to compute the averages of moments of fluctuating voltages and to reduce the averages and moments up to the third order of the fluctuating velocities.

The probes were traversed across the wake at stations $x = 1.6$, 12.7, 25.4, 51, 102 and 203 mm. The results at the first station $x = 1.6$ mm were sufficiently close to the trailing edge so that they could, excluding a few points very close to the centreline, be considered to be the boundary layers at the trailing edge.

3. Results

3.1. *Flow conditions*

Owing to the apparent sensitivity of near wake flows to such parameters as the details of the trailing-edge geometry, the scales and the state of the boundary layers at the trailing edge and the test conditions including the two-dimensionality, pressure gradient and the free-stream turbulence, it is useful to document the general flow properties before discussing the effects of the Reynolds number. First, the state of the boundary layers at the trailing edge may be judged from the values of the skin-friction coefficient C_f and the wake parameter of Coles (1962). The friction velocity u_τ and C_f were determined by fitting the logarithmic portion of the mean-velocity profiles at the first measurement station (1.6 mm downstream of the trailing edge) by the log-law with $\kappa = 0.41$ and $C = 5.2$ as recommended by Brederode & Bradshaw (1974). They are plotted in figure 3 against the Reynolds number R_θ. These plots indicate that the boundary layers at the trailing edge are close to the 'normal' flat-plate boundary layers at low Reynolds numbers.

The static pressure in the test section was found to be constant within $\pm 0.3\%$ of the test-flow dynamic pressure. This is of the order of magnitude of blockage caused by the 3 mm thick plate in a 550 mm high tunnel. The magnitude of viscous–inviscid interaction is related to $\mathrm{d}\delta^*/\mathrm{d}x$ which, in the range of the present experiments, varies between 0.003 and 0.002 and is much smaller than the pressure gradient due to the finite-angle trailing edge whose slope is $\tan(1.2°) = 0.02$. Hence the non-uniformity of the pressure field is mostly due to the tunnel and model geometry and not the viscous–inviscid interation. The variation of the momentum thickness in the wake was less than $\pm 2\%$ of the average value, θ. The average values are used in the presentation of results. A summary of the overall flow parameters is given in table 2.

3.2. *Mean-velocity results*

Figure 4 shows the development of the wake centreline velocity of some of the results from the present experiments. The present results verify that the trend suggested by the data shown in figure 1 is genuine. There is some difference between the data of figure 1 and the present data with similar values of R_θ. It can be due to any of many factors, including the differences in the upstream boundary layers, differences in the detailed trailing-edge geometry, influence of three dimensionality and measurement

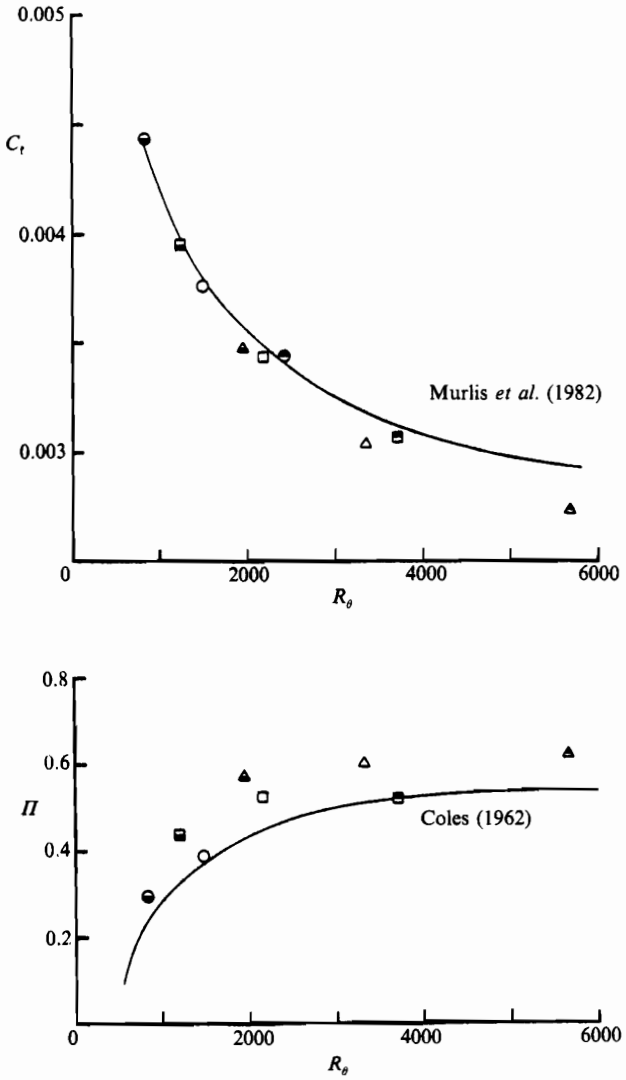

FIGURE 3. C_f and Coles' wake parameter at the trailing edge; symbols as in table 1.

methods and even the way u_τ is determined. The influence of the trailing-edge thickness, for example, was found to be significant near the trailing edge and it changes the slope of $U_c/u_\tau - u_\tau x/\nu$ curve. Figure 5 compares the results obtained with the model with a slightly thickened trailing edge and those of the original model under the same conditions. The thickness of the thickened trailing edge is 0.3 mm or $19\nu/u_\tau$ and is slightly larger than the viscous sublayer thickness. It is seen that for the thickened trailing edge, the velocity close to the trailing edge is reduced significantly but at positions further downstream of $x^+ > 2000$, the differences are negligible resulting in the increased slope of the $U_c/u_\tau - u_\tau x/\nu$ curve. For the present symmetric wakes, the thicker trailing edge may be thought to move the 'effective' trailing edge or the 'virtual origin' for the wake more downstream from the actual trailing-edge location.

Case name	STN1 $x =$ 1.6 mm x^+	STN2 $x = 12.7$ *mm* x^+	STN2 U_c/U_e	STN2 δ_i/θ	STN3 $x = 25.4$ mm x^+	STN3 U_c/U_e	STN3 δ_i/θ	STN4 $x = 50.8$ mm x^+	STN4 U_c/U_e	STN4 δ_i/θ	STN5 $x = 101.6$ mm x^+	STN5 U_c/U_e	STN6 $x = 203.2$ mm x^+	STN6 U_c/U_e
L10U40	55	464	0.593	0.93	923	0.650	1.33	1912	0.707	2.20	3711	0.754	7423	0.805
L10U80	101	870	0.611	1.14	1702	0.658	1.56	3395	0.706	—	6741	0.756	13530	0.810
L10U160	182	1554	0.629	1.09	3076	0.671	1.66	6111	0.729	2.40	12288	0.770	24462	0.820
L20U40	52	437	0.568	0.94	888	0.622	1.17	1776	0.675	2.12	3481	0.724	7175	0.775
L20U80	94	797	0.588	0.87	1594	0.632	1.22	3295	0.683	2.02	6508	0.727	13215	0.782
L20U160	173	1468	0.609	0.91	2921	0.653	1.21	5896	0.692	1.97	11810	0.739	23640	0.802
L40U40	49	411	0.528	0.56	824	0.582	0.86	1703	0.628	1.22	3263	0.682	6871	0.736
L40U80	90	765	0.545	0.52	1531	0.591	0.84	3042	0.639	1.28	6050	0.689	12467	0.739
L40U160	160	1365	0.568	0.59	2705	0.616	0.94	5402	0.661	—	10819	0.756	21510	0.753

Symbols in figures

7, 9, 10, ○ ($y > 0$) □ △ ▽ ◇

11, 14, 15 ○ ($y < 0$) □ △ ▽ ◇

† Turbulence data of case L40U40 were taken at $x = 95.3$ mm.

TABLE 2. Mean-flow parameters

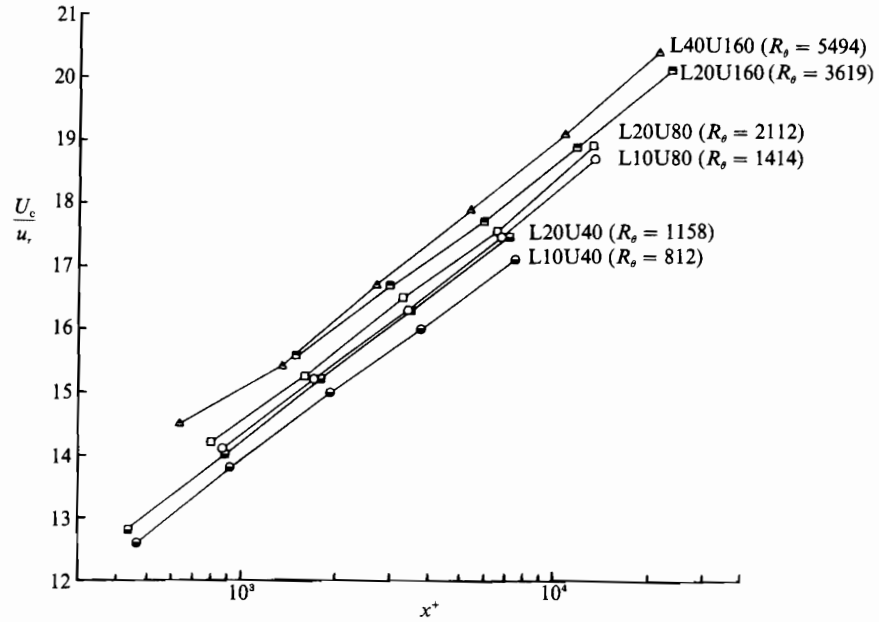

FIGURE 4. Wake centreline velocity; symbols as in table 1.

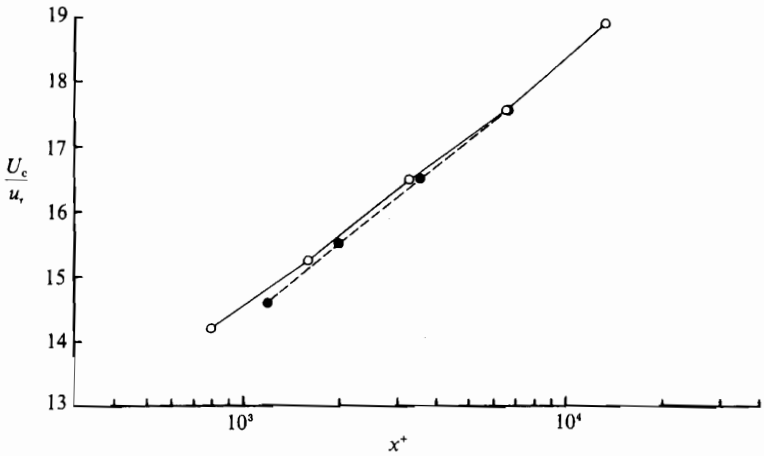

FIGURE 5. Effects of trailing-edge thickness on the development of centreline velocity: —○—, L20U80, trailing-edge thickness less than 0.05 mm; --●--, trailing-edge thickness 0.3 mm.

The Reynolds-number dependence indicated by the wall-variable scaling of figure 4 is seen to persist for much longer distances than the effects of trailing-edge geometry: the value of x/θ at $x^+ = 4000$ for the shortest model at the lowest free-stream velocity is about 100, which is large enough to be considered a far wake (Ramaprian *et al.* 1982). Since the difference does not diminish with the streamwise distance, it is not possible to absorb it by the introduction of the virtual origin to replace the actual trailing-edge position as could be done for the trailing-edge thickness effects.

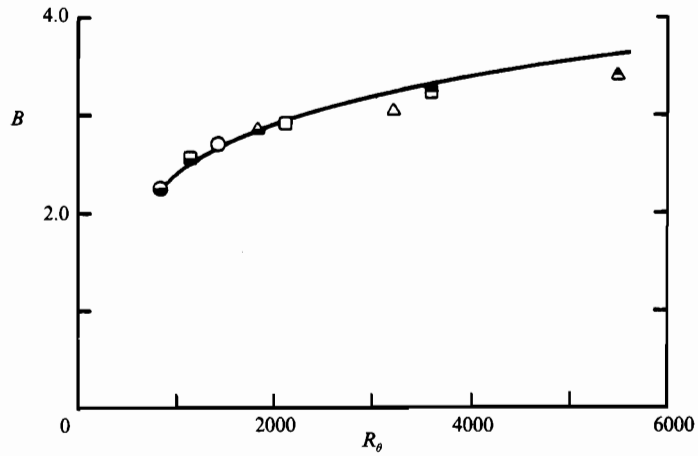

FIGURE 6. Variation of constant B with respect to Reynolds number R_θ, symbols as in table 1.

The way $U_c^+ \equiv U_c/u_\tau$ varies with $x^+ \equiv xu_\tau/\nu$ is seen to be described by the logarithmic function

$$U_c^+ = A \log_{10} x^+ + B, \tag{1}$$

reasonably accurately as found by Andreopoulos & Bradshaw (1980), who give the best fitting values of A and B to be 4.65 and 0.7, respectively. The data of Haji-Haidari & Smith (1988), which required an adjustment of u_τ to fit this equation with these values for the constants, are clearly influenced by the large trailing-edge angle. Their data are more like airfoil wake data. Nakayama (1984) shows that the slope A increases sharply for airfoils with angles of attack. The present results indicate that constant slope $A = 3.8$ fits most of the data including that of Andreopoulos & Bradshaw. The values of the intercept B appear to be a function of the Reynolds number and are plotted in figure 6 against R_θ. It is seen that B increases from about 13.5 to slightly above 15 as R_θ is increased from about 500 to 6000. The variation is about 10% and is significant. It should be stressed that A and B depend on many factors such as the trailing-edge thickness and perhaps the trailing-edge included angle and the values found here should not be taken as universal. Also for the present range of x^+ the data are fitted with equation (1), the increased slope A can be cancelled by the reduced intercept B. The relative variation of B for fixed A, however, can be considered to be more universally applicable.

Examples of complete velocity profiles are shown in figure 7 for $R_\theta = 1414$. The velocity profiles of all the cases measured are given in a report (Nakayama & Liu 1988). In this plot, both upper and lower halves of the wake are plotted to show the attained degree of symmetry. Points below $y^+ \equiv yu_\tau/\nu = 10$ are shown at $y^+ = 10$. Like the existing data of mean velocities in the near wake of flat plates, it is seen that the rapid mixing occurs in the central interaction region (the inner wake) and the outer parts remain practically unchanged at least up to the position $x/\theta \approx 50$. The extent of the inner wake can be identified as the region where the velocity profile deviates from the boundary-layer-wall-law profile, and in the following this position will be indicated by $y = \delta_i$. This definition of the inner wake edge is different from that of Andreopoulos & Bradshaw (1980) which is based on the intermittency of heated fluid coming from one side of the plate. At downstream positions, the changes

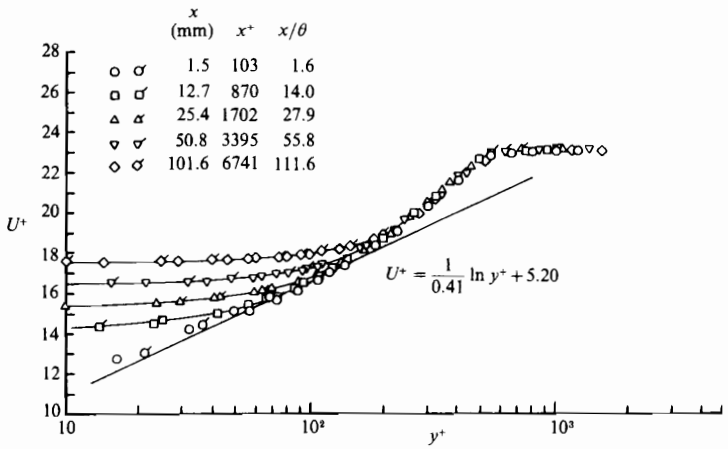

FIGURE 7. Mean-velocity profiles for the case $R_\theta = 1414$; symbols as in table 2.

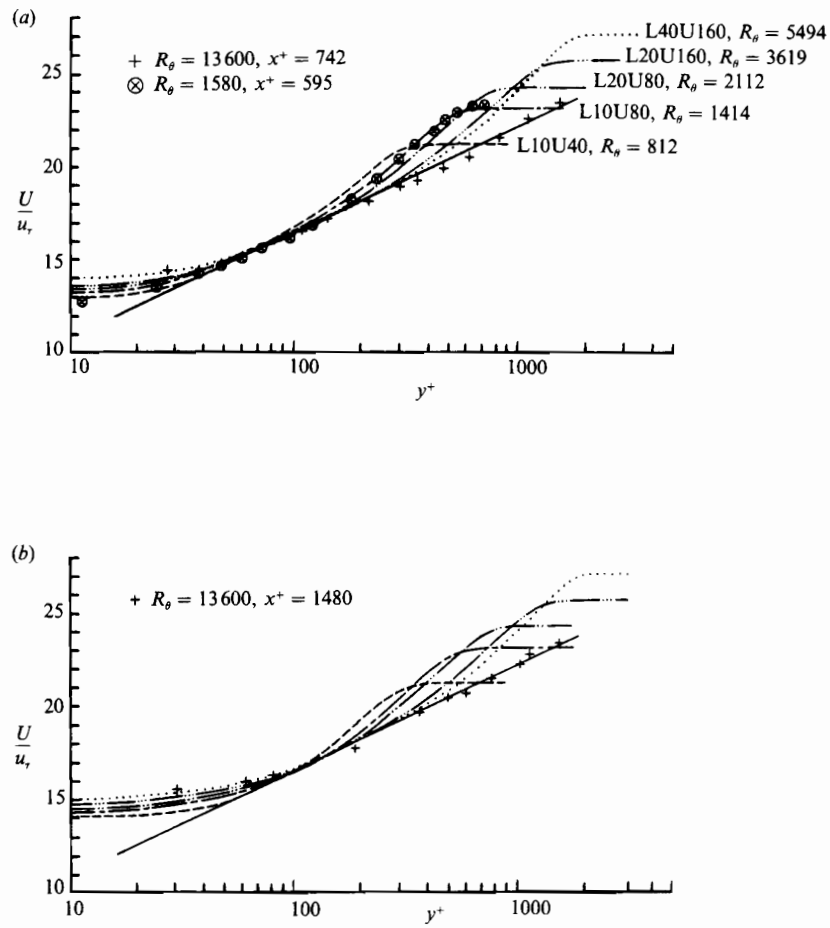

FIGURE 8(*a*,*b*). For caption see facing page.

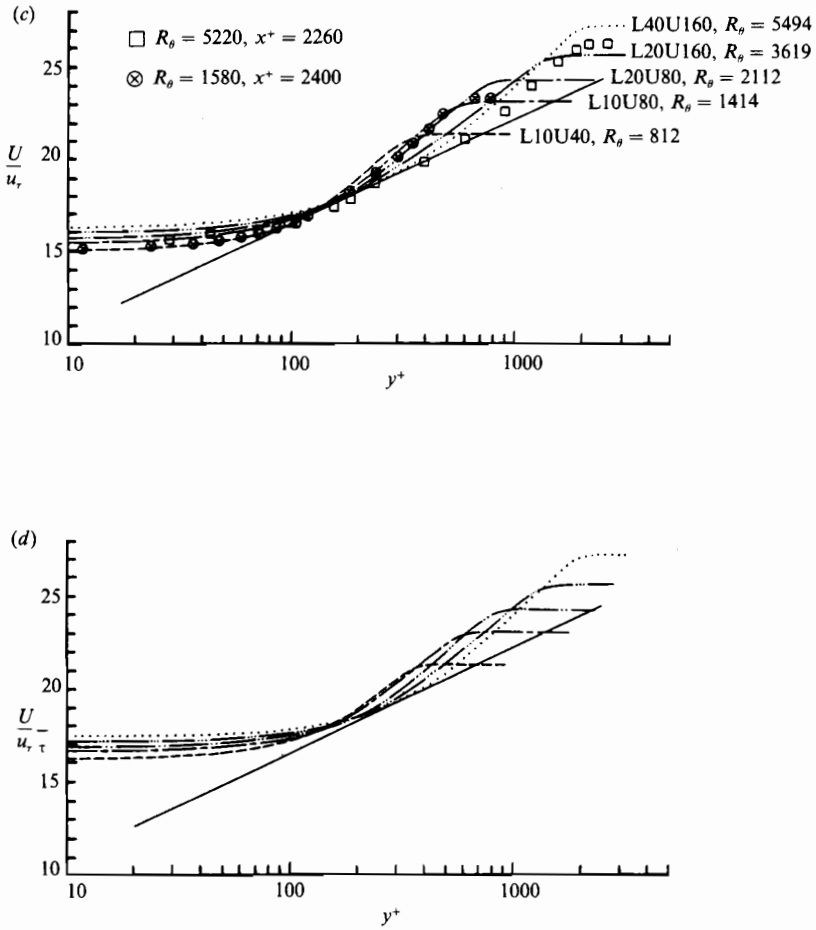

FIGURE 8. Velocity profiles interpolated at fixed x^+. (*a*) $x^+ = 500$; (*b*) $x^+ = 1000$; (*c*) $x^+ = 2000$; (*d*) $x^+ = 4000$; +, data of Andreopoulos & Bradshaw (1980); ⊗, data of Chevray & Kovasznay (1969); □, data of Ramaprian *et al.* (1982).

are gradual. This means that the outer layers of the near wake depend on the Reynolds number just like the outer layers of boundary layers. It is also seen that the log-law profile continues to exist at least up to about $x^+ = 2000$. Since the log-law profiles are independent of the Reynolds number and the log region is a kind of boundary condition for the development of the inner wake, it is not immediately obvious how the development of the centreline velocity depends on the Reynolds number.

The rest of the mean-velocity data are presented in figure 8 in the same inner-law coordinates interpolated at constant x^+ stations for different Reynolds numbers. The data of Chevray & Kovasznay (1969), Andreopoulos & Bradshaw (1980) and Ramaprian *et al.* (1982) are shown in appropriate parts of the figures for comparison with the present results. These existing data do fit with the results of the present series of measurements.

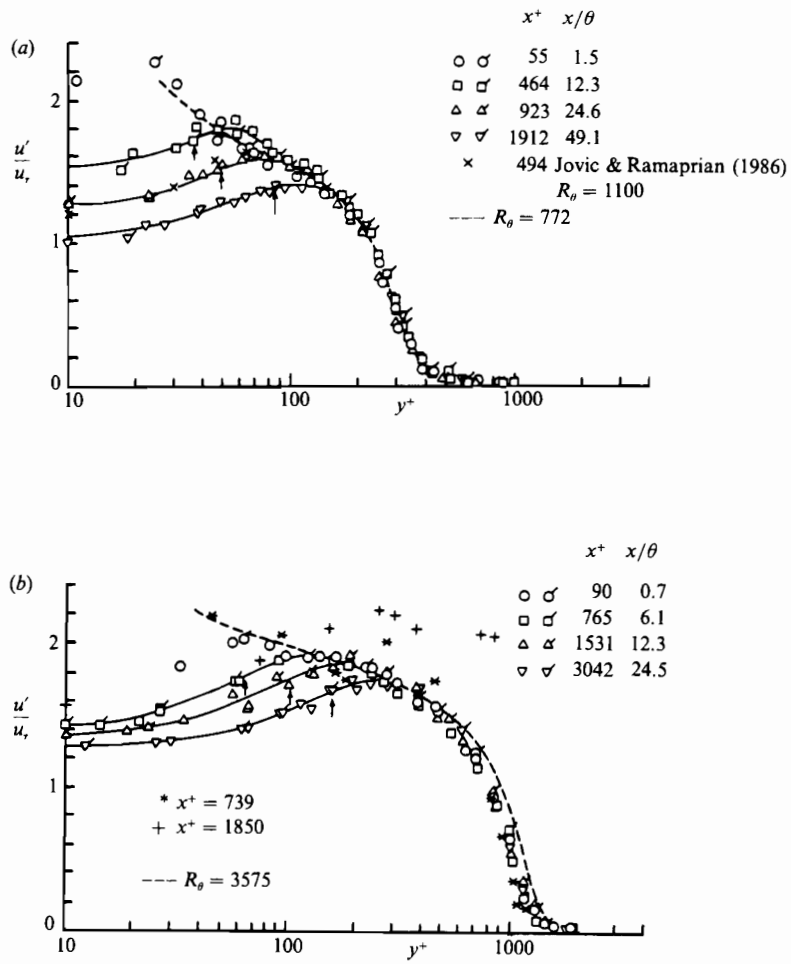

FIGURE 9. Streamwise turbulence intensity. (*a*) Case L10U40, $R_\theta = 812$; (*b*) Case L40U80, $R_\theta = 3213$; symbols for the present data are as in table 2; ---, boundary-layer data of Erm *et al.* (1985); *, data of Pot (1979); +, data of Andreopoulos & Bradshaw (1980); ↑, $y = \delta_1$.

3.3. *Turbulence quantities*

Detailed turbulence data were obtained in several test cases. Figures 9 and 10 show streamwise and transverse turbulence intensities $u' \equiv (\overline{u^2})^{\frac{1}{2}}$ and $v' \equiv (\overline{v^2})^{\frac{1}{2}}$, respectively at two Reynolds numbers, $R_\theta = 812$ and 3213. They are normalized by u_τ plotted against the wall coordinate $y^+ \equiv u_\tau y/\nu$ in the logarithmic scale in order to magnify the wake central region. Data at other Reynolds numbers are reported in Nakayama & Liu (1988). They also show the results of two different cases with nearly the same Reynolds numbers obtained with different size plates and velocity. The data from two sides of the wake are shown in order to give an idea of the symmetry and accuracy of the data. The hot-wire sensor length and the × -wire separation relative to the viscous scales, lu_τ/ν and su_τ/ν are about 30 and 60 for $U_\infty = 12$ and 24 m/s, respectively, so that the data very close to the trailing edge in the first measurement station $x = 1.6$ mm may be influenced by the problem of finite size effects (Nakayama

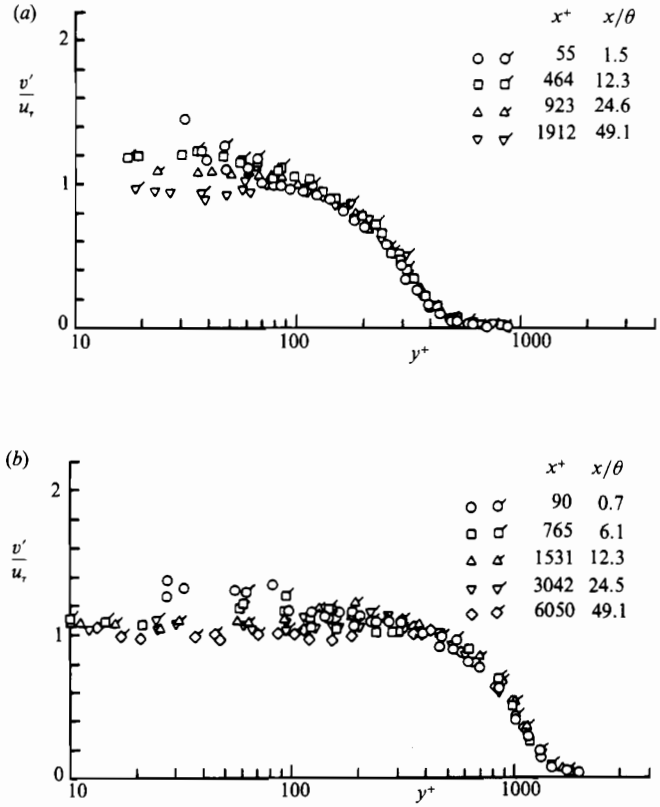

FIGURE 10. Transverse turbulence intensity. (*a*) $R_\theta = 812$; (*b*) $R_\theta = 3213$; symbols as in table 2.

& Westphal 1986). The high level of v' near the wake centre at $x = 1.6$ mm station may be due to the sensor separation. The magnitudes of these sensor size effects are expected to be smaller than 5%.

The existing flat-plate data of Chevray & Kovasznay (1969), Andreopoulos, Durst & Jovanovic (1983), Pot (1979) and Jovic & Ramaprian (1986) are shown in appropriate parts of the figures for comparison. The flat-plate boundary-layer data of Erm *et al.* (1985) are also shown since their measurements were done at closely spaced Reynolds numbers so that results corresponding to the Reynolds numbers of the present experiments can be extracted. Generally, the present results and the available data are compatible and agree well. The data of Ramaprian *et al.* (1982), and the shear-stress data of Pot (1979), which show large peaks in the near wake owing possibly to vortex shedding from their rather thick trailing edge, are omitted, to avoid confusion.

The arrows in figure 9 indicate positions $y^+ = \delta_i^+ \equiv u_\tau \delta_i/\nu$. It is seen that u' rapidly decreases in the region $y^+ \leqslant \delta_i^+$, while v' changes very little with the distance from the trailing edge. It is also seen that the reduction in u' is distinct and is related to the inner-wake width as determined from the mean velocity profiles. The region where u' is influenced, however, is seen to be consistently wider than the region where the mean velocity is influenced by the merging of the two boundary layers.

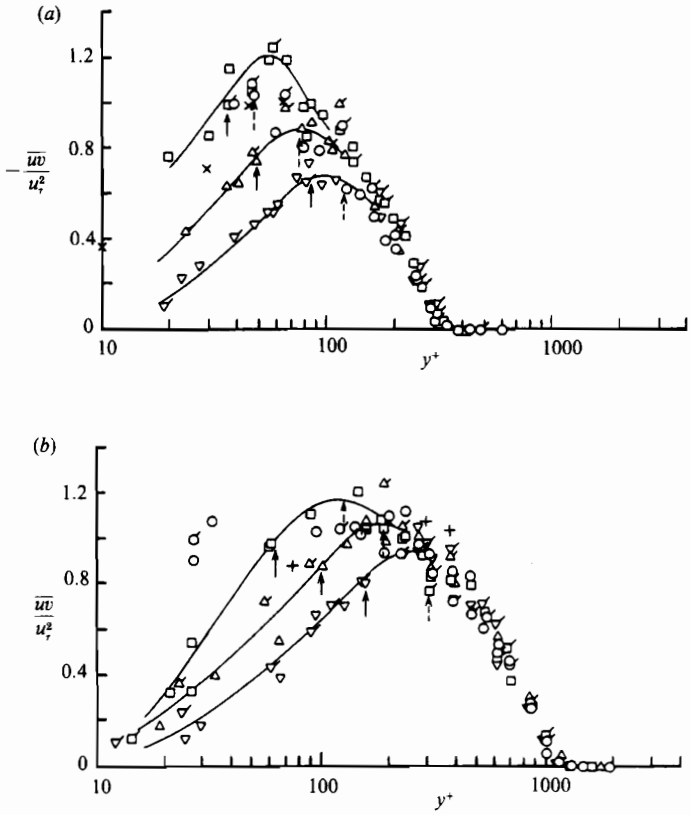

FIGURE 11. Turbulent shear stress. (*a*) Case L10U40, $R_\theta = 812$; (*b*) Case L40U80, $R_\theta = 3213$; symbols as in table 2; ↑, $y = \delta_1$; ↑, $y = \delta_1'$.

Figure 11 shows the results of the turbulent shear stress $-\overline{uv}$, plotted in a similar way to u' and v'. The data from the lower half of the wake, $y < 0$, are plotted with the signs of both $-\overline{uv}$ and y reversed so that they can be readily compared with the data in the upper half. Solid arrows and dotted arrows indicate the edges of the region where the mean velocity and the turbulence u', respectively, are affected by the boundary layer merging. It is seen that $|-\overline{uv}|$ is influenced over a wider region than the mean velocity or u'. The fact that there are differences in the widths of the layers that the mean velocity, u' and $|\overline{uv}|$ are deviated from their respective boundary-layer profiles implies that the present definition of the inner-wake thickness is not a unique one and different from that of Andreopoulos & Bradshaw (1980).

It is seen that the maximum value of $|-\overline{uv}|/u_\tau^2$ at the first two stations are higher than 1, particularly at the second station, it is almost 1.2. The finite sensor size effects of the hot-wire probe cannot be the reason since, as found in Nakayama & Westphal (1986), their effects on the shear stress are almost negligible compared with those on the normal stresses which were found to be only about 5% or less. The slight adverse pressure gradient induced by the non-zero trailing-edge angle, at best can account for an overshoot of only 5%. The results at the first station show a small overshoot of about this magnitude and may be considered to be due to the pressure gradient, but

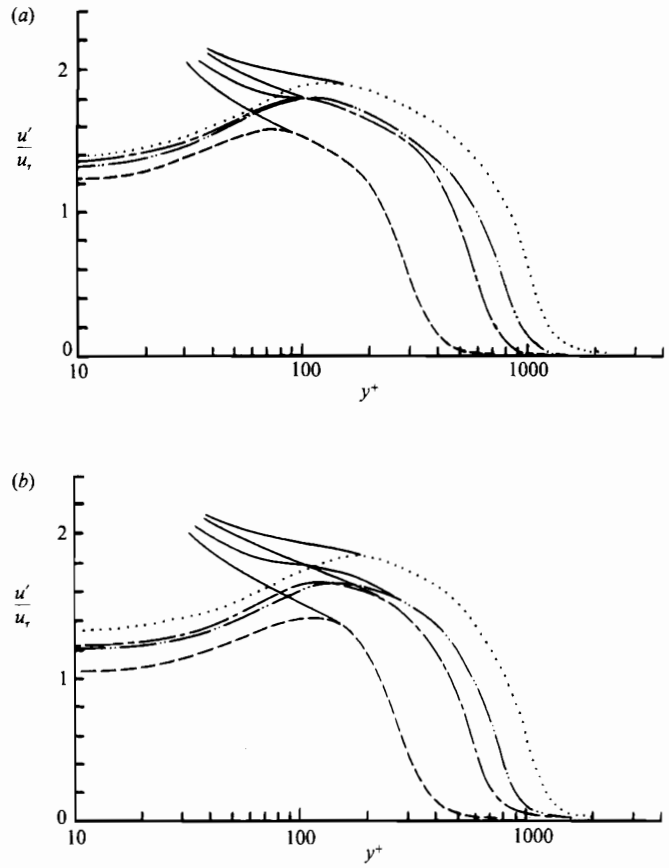

FIGURE 12. Streamwise turbulence intensity interpolated at constant x^+. (*a*) $x^+ = 1000$; (*b*) $x^+ = 2000$; ---, $R_\theta = 812$; ——, $R_\theta = 1845$; —·—, $R_\theta = 2112$; ···, $R_\theta = 3213$.

a much larger peak value at the next station can only be explained as a near-wake phenomenon. All of the available wake data except for those of Chevray & Kovasznay (1969), show increases in the peak shear stress just downstream of the trailing edge. The data that are obviously influenced by a thick trailing edge (Pot 1979; Ramaprian *et al.* 1982) show even larger and peakier overshoots.

In order to show the trend with respect to the Reynolds number in terms of wall coordinates, data are interpolated at fixed x^+ as done with the mean-velocity data. Figure 12(*a*, *b*) shows the u' profiles interpolated at $x^+ = 1000$ and 2000, respectively. Figure 13(*a*, *b*) shows the corresponding $-\overline{uv}$ profiles. The extension into the wake central region indicated by the solid lines is the result at the trailing edge. Since figure 10 indicates that v' changes very little, a separate plot is not made. Figure 12 indicates that u' at a fixed x^+ position generally increases with higher Reynolds number. The outer layers are practically unchanged from the boundary layers at the trailing edge, and the Reynolds-number effects are also the same as in the outer layer of a boundary layer. Unlike the case of mean-velocity profiles, there is no region that is independent of R_θ. It is partly due to the fact that the range of y^+ in which there is a log-law similarity is dependent on R_θ (see figure 8), and also due to the fact that

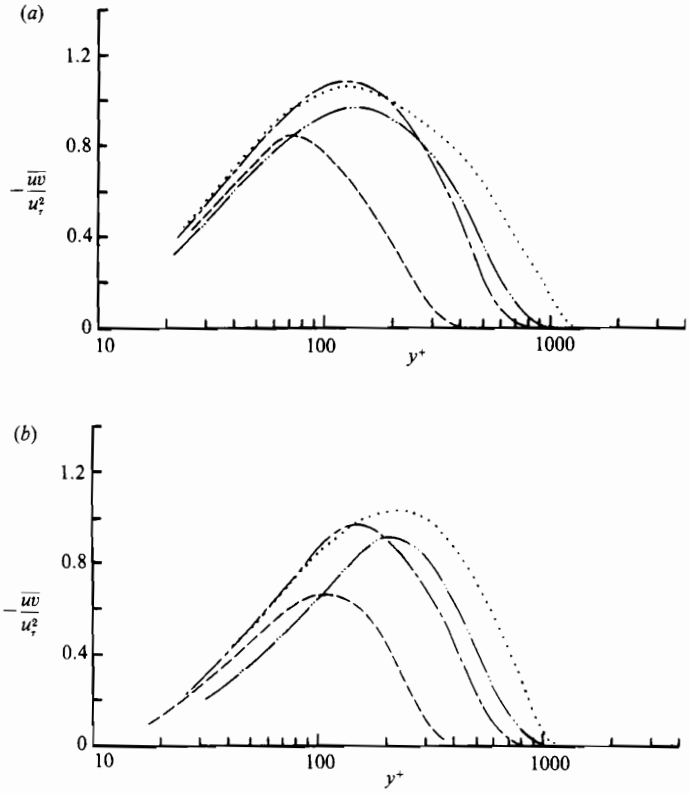

FIGURE 13. Turbulent shear stress interpolated at constant x^+. (*a*) $x^+ = 1000$; (*b*) $x^+ = 2000$; lines are as in figure 12.

u' in the inner layer of the boundary layer is already slightly R_θ dependent (see the data of Erm *et al.* 1985). Although some uncertainties are apparent in the shear-stress results owing to larger measurement errors, essentially the same trend but less pronounced as u' with respect to R_θ is seen.

The distributions of the triple products $\overline{u^2v}$ and $\overline{uv^2}$ are plotted in figures 14 and 15, respectively, in the same way as the turbulent shear stress is plotted in figure 12. $\overline{u^2v}$ is supposed to be antisymmetric around $y = 0$ and the data from the lower side of the wake is plotted with the sign reversed. The accuracies of these quantities are expected to be poorer than the lower-order quantities and there is more scatter among data points. The only available data of the triple products are those of Andreopoulos (1978) and Jovic & Ramaprian (1986) and they are inserted in the appropriate parts of the figures. The data of Jovic & Ramaprian, which are obtained at Reynolds number in the range of the present experiments, agree well with the present results at similar positions and at similar Reynolds numbers. Andreopoulos' data have been obtained at a Reynolds number much higher than those of the present results and show somewhat different behaviour. The minimum in the $\overline{u^2v}$ profile is considerably lower and the maxima in $\overline{uv^2}$ profiles are much higher than the present low-Reynolds-number cases. The general trend of the present data is that the wake centre region, where these triple products have the opposite sign to those in the

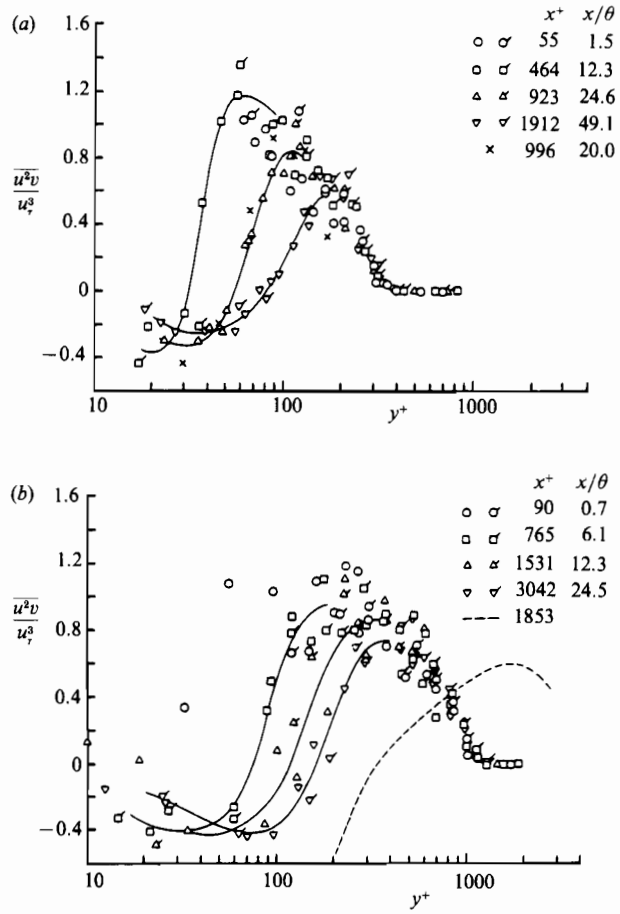

FIGURE 14. Triple product $\overline{u^2v}$. (*a*) Case L10U40, $R_\theta = 812$; (*b*) Case L40U80, $R_\theta = 3213$; symbols for the present data are as in table 2; ---, data of Andreopoulos (1978), $R_\theta = 13600$; ×, data of Jovic & Ramaprian (1986); the solid-line curves are for visual side only.

outer layer, is wider for higher Reynolds numbers, but the magnitudes of the triple products do not vary very much. The position where the triple products containing v change sign is the point where the y-component transport of the corresponding Reynolds stresses changes direction. This region is the stress-producing region and its position appears Reynolds-number dependent.

4. Discussion

4.1. *Reynolds-number effect on the mean-velocity profile*

The present result makes it clear that the development of the wake centreline velocity in terms of the inner-law scaling depends on the Reynolds number, R_θ, in the range covered by the present work, in which the boundary layer at the trailing edge is fully-turbulent but considered a 'low-Reynolds number' boundary layer according to Coles (1962). Other scales involving outer lengthscales and defect-velocity do not either collapse the data or improve correlation (Nakayama & Liu

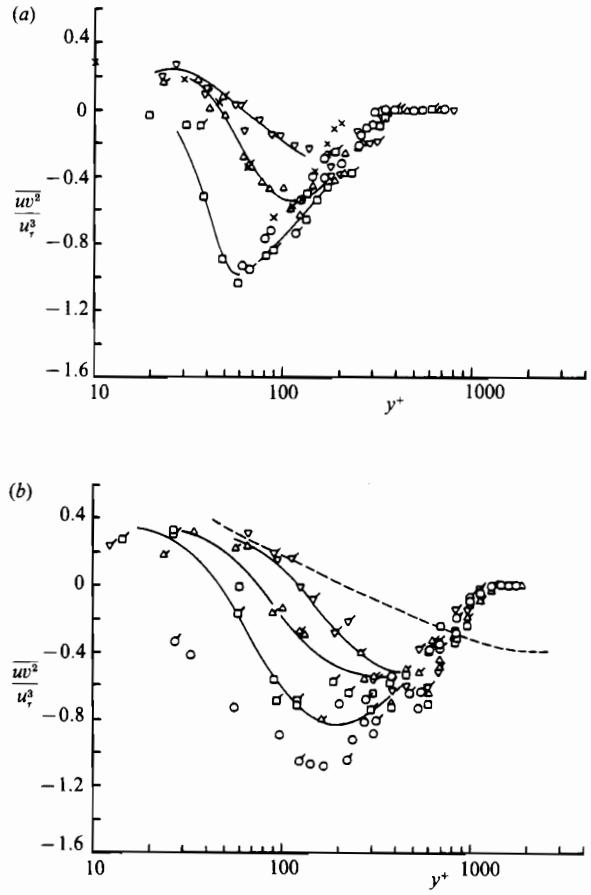

FIGURE 15. Triple product $\overline{uv^2}$. (*a*) $R_\theta = 812$; (*b*) $R_\theta = 3213$; symbols are as in figure 14.

1988). It should be noted, however, that the development of the entire velocity profiles, as shown in figure 8, clearly indicate that the logarithmic similarity of the upstream boundary layer, which is independent of R_θ, continues to exist at least up to $x^+ = 2000$ for the lowest Reynolds number ($R_\theta = 812$) and much larger x^+ for the highest R_θ. Hence in significant portions of the range of x^+ shown in figure 4, there is the inner-law similarity in part of the profile. Therefore, the inner-law scaling provides the most convenient reference and the data are best interpreted in terms of the deviation from the log-law. This was the basic approach of Coles (1962) in the development of the concept of the 'wake function' and the low-Reynolds-number effects in the zero-pressure gradient boundary layer.

Figure 16 is an illustration of what the data imply about the way the velocity profiles in the wake change with respect to R_θ, in terms of the inner-law scaling. As R_θ is reduced, the 'wake component', which is the deviation from the log-law in the outer layer, decreases just like the boundary layer. At the same time, the deviation in the inner wake decreases. As the position of the wake component shifts inward with decreasing R_θ, the edge of the inner wake also moves inward. The log-law, as long as it exists, is uninfluenced but the range of y^+ over which it is valid shrinks and

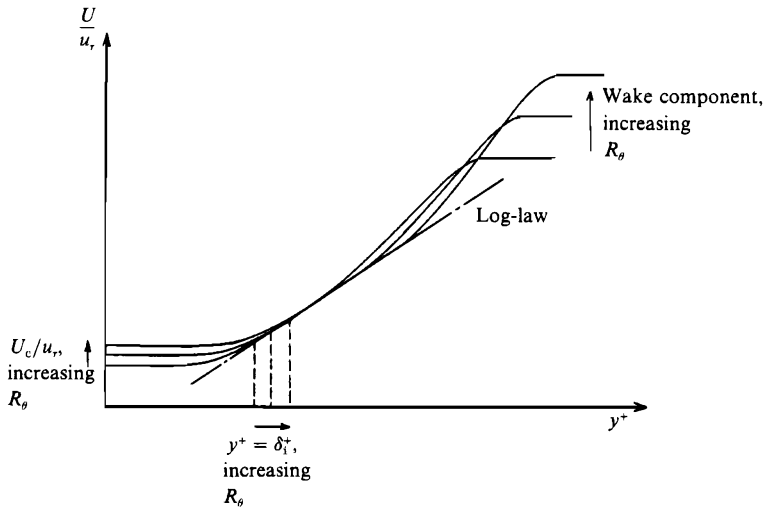

FIGURE 16. Effects of R_θ on the mean-velocity profiles.

shifts to the lower y^+. For Reynolds numbers lower than the present lower limit, the region of the log-law similarity will further diminish and the present way of interpreting the profiles will be difficult.

The reason why the wake component shifts inward for lower R_θ is because it is a property of the outer-layer eddies which scale with δ, or the outer-layer scale. The fact that the width of the inner layer decreases with R_θ suggests that δ_i may also be correlated with the outer-layer scales. The spread of the inner wake occurs both by the local mixing by the small-scale motions and by the large-scale undulation of the instantaneous positions of the interface between the flows from two sides of the plate. For small δ_i/δ, Bradshaw (1970) assumed the former is dominant and used ν/u_τ to scale it. If the large-scale undulations are significant, which, in fact, is an implication of the flow-visualization of Maekawa & Nozaki (1986) and Haji-Haidari & Smith (1988) indicating that the large structures of the boundary layers start to cross over the centreline causing the flapping of the streaks of the low-speed fluid, δ_i would be influenced by the outer-layer scales as well. Figure 17 indicates that δ_i is correlated well with θ for all Reynolds numbers covered. According to Townsend (1961) and Bradshaw (1967) the eddies in the outer layer do induce motion in the inner layer, but in the wall-bounded boundary layers, they are mainly in u and w and do not contribute to v or uv and hence do not influence U. Therefore, they are 'inactive' and the local 'active' motions with inner scales contribute to the universality of the inner layer. In the wake, the restriction on the v component is removed so that stronger influence of the outer-layer eddies, and hence the outer-layer scales, through enhanced v and uv is naturally anticipated. The present data do indicate that v' increases, but figure 10 shows that this increase is limited to the region just downstream of the viscous sublayer of the boundary layer where v' is small (figure 10 does not contain data in the viscous sublayer), and in the rest of the wake there is practically no change. Hence, the induced motion may be thought to become 'active' only in the wake centreline regions, leaving the log-law region still uninfluenced by the induced motion.

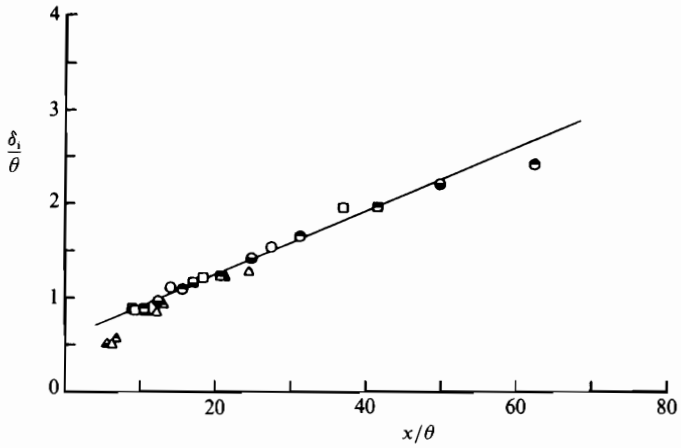

FIGURE 17. Development of inner-wake width; symbols as in table 1.

4.2. *Reynolds-number effects on the turbulent stresses*

Unlike the mean-velocity profiles that grow slowly from those of the boundary layer, the turbulent stresses show two types of changes. The first one is the step change occurring over a short distance, presumably of the order of a few viscous sublayer thicknesses, downstream of the trailing edge. Measurements by Haji-Haidari & Smith (1988) made in the region very close to the trailing edge imply that this distance is about $100x^+$. This is the initial response to the sudden loss of the wall, i.e. the sudden loss of the non-slip boundary condition on the instantaneous velocity. The second type is the slow development that takes place over much of the streamwise extent covered by the present measurements.

The first type of change occurs so suddenly that it is a local phenomenon, and it scales with the inner-layer variables and is R_θ-independent. v', normalized by u_τ in the inner wake and even in the log-law region, is remarkably constant (≈ 1.1) for all R_θ (see figure 10). This implies that the magnitude of the transverse velocity v, resulting from the removal of the wall, is independent of R_θ and is very nearly equal to u_τ. The sudden drop of the shear stress from the boundary-layer value to the wake centreline value is, of course, one to zero for all R_θ. The data of u' as plotted in figure 12, show some R_θ dependency, but for small x^+, say $x^+ < 1000$, the variation is small. It follows that in the close neighbourhood of the trailing edge, the turbulent stresses are independent of R_θ in the inner-law scales. However, the type of low-Reynolds-number effects on the turbulence models needed for the near-wall region of boundary layers (e.g. Patel *et al.* 1985) would exist in this region.

From the inner-scale plots of figures 12 and 13, the way the turbulent stresses develop after the above-described initial R_θ-independent responses have taken place is seen to depend on R_θ. Figure 12 definitely indicates that u'/u_τ inside the inner wake is lower for lower R_θ and more so at larger x^+ so that the gradient is larger. Figure 13 shows that the peak value of $|\overline{uv}|/u_\tau^2$ is smaller for lower R_θ if compared at the same x^+. The way that the slowly varying part of the turbulent stresses depends on R_θ is consistent with the concept of the effects of the outer-layer eddies. The outer-layer eddies are larger for larger R_θ and hence their influence is larger.

The significance of the R_θ dependence of the turbulent stresses should perhaps be

examined based on the equation of motion, which near the wake centreline reduces to

$$U_c^+ \frac{dU_c^+}{dx^+} = \frac{\partial}{\partial x^+}\left(\frac{\overline{u^2}-\overline{v^2}}{u_\tau^2}\right)+\frac{\partial}{\partial y^+}\left(\frac{-\overline{uv}}{u_\tau^2}\right). \tag{2}$$

It has been seen that dU_c^+/dx^+ is more or less independent of R_θ and hence the relative change of the left-hand side of this equation with respect to R_θ is the same as U_c^+. The right-hand side must also change like U_c^+ but its variation over the presently covered range of R_θ, is not much larger than the scatter and error in the turbulence data so that the precise way that the balance of momentum is influenced by R_θ may not be evaluated. However, the magnitude and the variation of the normal-stress terms are as large as the variation of U_c with respect to R_θ, at least up to $x^+ = 1000$. Hence, it is important to include the normal-stress terms in order to reflect the Reynolds-number effects.

5. Conclusions

Measurements in the near wake of flat plate models were made by varying the Reynolds number in order to investigate low-Reynolds-number effects in this region. The results indicate that some of the discrepancies in the existing mean-velocity data are due to differences in the Reynolds number. It was found that, while the inner-law similarity continued to exist in the near wake, the width of the inner wake scaled with the outer variable and hence depended on R_θ. This is an indication of a stronger influence of outer-layer large eddies on the inner part of the wake compared to the inner layer of the wall-bounded boundary layers. The mean velocity along the centreline was found to be smaller for lower Reynolds number but the mean flow within the inner wake was approximately self-similar.

The trends of the turbulent stresses in the outer wake with respect to Reynolds number are similar to the low-Reynolds-number effects in the outer layer of boundary layers. Inside the inner wake, the streamwise turbulence intensity is lower for lower Reynolds numbers but the transverse fluctuations are nearly constant. The turbulent shear stress profiles show similarity if scaled with u_τ^2 and plotted against y/δ_i.

This work was conducted at California State University, Long Beach and was supported by National Science Foundation Grant MEA-8018565.

REFERENCES

AKDAG, V. 1983 An experimental investigation of a wake merging into a boundary layer in constant pressure. MS thesis, Dept of Mech. Engng, California State University, Long Beach.

AKDAG, V., NAKAYAMA, A., LIU, B., KILIK, E. & UNT, H. 1984 Automated hot-wire measurements using a micro computer. *Rep.* ME84-5, Dept of Mech. Engng, California State University, Long Beach.

ALBER, I. E. 1980 Turbulent wake of a thin flat plate. *AIAA J.* **18**, 1044–1051.

ANDREOPOULOS, J. 1978 Symmetric and asymmetric near wake of a flat plate. PhD thesis, Imperial College of Science and Technology, London.

ANDREOPOULOS, J. & BRADSHAW, P. 1980 Measurements of interacting turbulent shear layers in the near wake of a flat plate. *J. Fluid Mech.* **100**, 639–668.

ANDREOPOULOS, J., DURST, F. & JOVANOVIC, J. 1983 On the structure of turbulent boundary layers at different Reynolds numbers. In *Fourth Symposium on Turbulent Shear Flows*, University of Karlsruhe, Karlsruhe, FRG, pp. 2.1–2.7.

BADRI NARAYANAN, M. A., RAGHU, S. & TULAPURKARA, E. G. 1985 The nonequilibrium region of a mixing layer. *AIAA J.* **23**, 987–991.

BOGUCZ, E. A. 1984 Analysis of the turbulent near wake at a sharp trailing edge. PhD dissertation, Lehigh University, Bethlehem, PA.

BOGUCZ, E. A. & WALKER, J. D. A. 1987 Analysis and prediction of the turbulent near wake at a sharp trailing edge. *AIAA paper* 87-0483.

BRADSHAW, P. 1967 'Inactive' motion and pressure fluctuations in turbulent boundary layers. *J. Fluid Mech.* **30**, 241–258.

BRADSHAW, P. 1970 Prediction of the turbulent near-wake of a symmetrical aerofoil. *AIAA J.* **8**, 1507–1512.

BREDERODE, V. A. S. L. DE & BRADSHAW, P. 1974 A note on the empirical constants appearing in the logarithmic law for turbulent wall flows. *I.C. Aero Rep.* 74-03, Imperial College of Science and Technology, London.

CEBECI, T. 1973 Kinematic eddy viscosity at low Reynolds numbers. *AIAA J.* **11**, 102–104.

CEBECI, T., THIELE, F., WILLIAMS, P. G. & STEWARTSON, K. 1979 On the calculation of symmetric wakes, I. Two-dimensional flows. *Numer. Heat Trans.* **2**, 35–60.

CHANG, K. C., BUI, M. N., CEBECI, T. & WHITELAW, J. H. 1986 The calculation of turbulent wakes. *AIAA J.* **24**, 200–201.

CHEVRAY, R. & KOVASZNAY, L. S. G. 1969 Turbulence measurements in the wake of a thin flat plate. *AIAA J.* **7**, 1641–1643.

COLES, D. E. 1962 The turbulent boundary layer in a compressible fluid. *RAND Corp. Rep.* R-403-PR.

ERM, L. P., SMITS, A. J. & JOUBERT, P. N. 1985 Low Reynolds number turbulent boundary layers on a smooth flat surface in a zero pressure gradient. *Fifth Symposium on Turbulent Shear Flows, Cornell University, Ithaca, NY*, pp. 2.13–2.18.

HAJI-HAIDARI, A. & SMITH, C. R. 1988 Development of the turbulent near wake of a tapered thick flat plate. *J. Fluid Mech.* **189**, 135–163.

JOVIC, S. & RAMAPRIAN, B. P. 1986 Large-scale structure of the turbulent wake behind a flat plate. *IIHR Rep. no.* 298, The University of Iowa, Iowa City.

MAEKAWA, H. & NOZAKI, T. 1986 Visualized large-scale motions in the turbulent wake behind a symmetrical airfoil. *Proc. 3rd Asian Congress of Fluid Mech., 1–5 Sept.* 1986, *Tokyo, Japan*, pp. 690–693.

MURLIS, J., TSAI, H. M. & BRADSHAW, P. 1982 The structure of turbulent boundary layers at low Reynolds numbers. *J. Fluid Mech.* **122**, 13–56.

NAKAYAMA, A. 1984 Measurements of attached and separated turbulent flows in the trailing-edge regions of airfoils. In *Numerical and Physical Aspects of Aerodynamic Flows, II* (ed. T. Cebeci), pp. 233–255. Springer.

NAKAYAMA, A. & LIU, B. 1988 Low-Reynolds number effects in the near wake of a flat plate. *California State University, Long Beach, Mech. Engng Dept Rep.* CAR-88-1.

NAKAYAMA, A. & WESTPHAL, R. V. 1986 The effects of sensor length and spacing on $\times$-wire measurements in a boundary layer. *NASA TM*88352.

PATEL, V. C. & CHEN, H. C. 1989 Turbulent wake of a flat plate. Submitted to *AIAA J.*

PATEL, V. C., RODI, W. & SCHEUERER, G. 1985 Turbulence models for near-wall and low Reynolds number flows: A review. *AIAA J.* **23**, 1308–1319.

POT, P. J. 1979 Measurements in a 2-D wake and in a 2-D wake merging into a boundary layer. *Data Report, NLR TR*-7900638, The Netherlands.

PURTELL, L. P., KLEBANOFF, P. S. & BUCKLEY, F. T. 1981 Characteristics of turbulence in a boundary layer with zero pressure gradient. *Phys. Fluids* **24**, 802–811.

RAMAPRIAN, B. R., PATEL, V. C. & SASTRY, M. S. 1982 The symmetric turbulent wake of a flat plate. *AIAA J.* **20**, 1228–1235.

SPALART, P. R. 1988 Direct simulation of a turbulent boundary layer up to $R_\theta = 1410$. *J. Fluid Mech.* **187**, 61–98.

TOWNSEND, A. A. 1961 Equilibrium layers and wall turbulence. *J. Fluid Mech.* **11**, 97–120.

WHITE, B. R. 1981 Low-Reynolds-number turbulent boundary layers. *Trans. ASME* I: *J. Fluids Engng* **103**, 624–630.